



ACADEMIC  
PRESS

Available online at [www.sciencedirect.com](http://www.sciencedirect.com)

SCIENCE @ DIRECT®

Icarus 163 (2003) 414–427

ICARUS

[www.elsevier.com/locate/icarus](http://www.elsevier.com/locate/icarus)

# HST observation of the atmospheric composition of Jupiter's equatorial region: evidence for tropospheric C<sub>2</sub>H<sub>2</sub><sup>☆</sup>

Yan Bétrémieux,<sup>a,\*</sup> Roger V. Yelle,<sup>b</sup> and Caitlin A. Griffith<sup>b</sup>

<sup>a</sup> *Scientific Solutions, Inc., 55 Middlesex Street, Unit 210, North Chelmsford, MA 01863-1561, USA*

<sup>b</sup> *Department of Planetary Science and the Lunar and Planetary Laboratory, University of Arizona, Tucson, AZ 85721, USA*

Received 13 June 2002; revised 17 January 2003

## Abstract

This paper presents the first detailed analysis of acetylene absorption features observed longward of 190.0 nm in a jovian spectrum by the Faint Object Spectrograph on board the Hubble Space Telescope. The presence of two features located near 207.0 nm can only be explained by a substantial abundance of acetylene in the upper troposphere. Using a Rayleigh–Raman radiative transfer model, it was determined that the acetylene vertical profile is characterized by a decrease in the mole fraction with increasing pressure in the upper stratosphere, a minimum around 14 to 29 mbar, followed by an increase to about  $1.5 \times 10^{-7}$  in the upper troposphere. Longward of 220 nm, the relatively high contrast of Raman features to the continuum precludes the existence of an optically significant amount of clouds from 150 to 500 mbar unless they are highly reflective. Instead, the reflectivity at these long wavelengths is determined by stratospheric, not tropospheric, scatterers and absorbers. Analysis of the data also suggests that ammonia is extremely undersaturated at pressures below 700 mbar. However, no firm conclusions can be reached because of the uncertainties surrounding its cross section longward of 217.0 nm, which are due to vibrationally excited states.

© 2003 Elsevier Science (USA). All rights reserved.

*Keywords:* Jupiter; atmosphere; Spectroscopy; Radiative transfer; UV observations

## 1. Introduction

Acetylene (C<sub>2</sub>H<sub>2</sub>) is a key constituent in the hydrocarbon photochemistry of the jovian atmosphere. It is produced in the upper stratosphere by a chain of photochemical reactions initiated by the photolysis of methane (CH<sub>4</sub>). Eddy mixing then transports acetylene downward deep into the atmosphere where it is converted back to methane (Strobel, 1969). Reaction of acetylene with the products of its own photolysis or with other hydrocarbon species leads to the formation of more complex hydrocarbons. These processes

eventually result in the production of polyacetylenes or polynes which are candidates for jovian aerosols (West et al., 1986). Furthermore, the coupled photochemistry of acetylene with ammonia (NH<sub>3</sub>) has been postulated (Kaye and Strobel, 1983) and verified in the laboratory (Ferris and Ishikawa, 1988) to lead to the formation of hydrogen cyanide (HCN).

Ultraviolet absorption features of acetylene have been observed shortward of 190.0 nm in jovian spectra. Many observations were accomplished with the International Ultraviolet Explorer (IUE) at low spectral resolution (approximately 1.0 nm) with the large aperture. C<sub>2</sub>H<sub>2</sub> was first detected in the ultraviolet spectrum of Jupiter by Owen et al. (1980). They deduced that C<sub>2</sub>H<sub>2</sub> could be uniformly mixed down to 80 mbar with a mixing ratio of  $2.2 \times 10^{-8}$ . Clarke et al. (1982), Gladstone and Yung (1983), Wagener et al. (1985), and McGrath et al. (1990) determined the C<sub>2</sub>H<sub>2</sub> mixing ratio in the stratosphere to be  $(0.6–1.8) \times 10^{-7}$ ,  $1 \times 10^{-7}$ ,  $3 \times 10^{-8}$ , and  $3.55 \times 10^{-8}$  respectively. Morrissey et

<sup>☆</sup> Based on observations made with the NASA/ESA Hubble Space Telescope, obtained from the data archive at the Space Telescope Science Institute, which is operated by the Association of Universities for Research in Astronomy, Inc., under NASA Contract NAS 5-26555.

\* Corresponding author. Fax: +1-978-251-8822.

E-mail address: [yan@sci-sol.com](mailto:yan@sci-sol.com) (Y. Bétrémieux).

<sup>1</sup> This work was accomplished at Boston University as part of Dr. Bétrémieux's Ph.D. dissertation.

al. (1995) obtained better resolution spectra (0.35 nm) of the jovian equatorial region with the Hopkins Ultraviolet Telescope (HUT) on two flights of the Space Shuttle. They derived  $C_2H_2$  mixing ratios of  $3.9 \times 10^{-8}$  and  $2.8 \times 10^{-8}$  and probed predominantly the 10-mbar region of the atmosphere.

Acetylene has also been observed in the infrared at different pressure levels. Sada et al. (1998) measured a mole fraction of acetylene of  $(1.8\text{--}2.8) \times 10^{-8}$  in the 1- to 40-mbar region while Noll et al. (1986) measured a mixing ratio of  $(0.7\text{--}1.3) \times 10^{-7}$  at about 1.5 mbar. Higher altitude measurements, by Yelle et al. (2001) and Bézard et al. (1997), yielded respectively a mole fraction of  $(2\text{--}3) \times 10^{-6}$  from 0.004 to 0.02 mbar and a mixing ratio of  $1 \times 10^{-5}$  from 2 to 6  $\mu$ bar. This observed increasing mixing ratio of  $C_2H_2$  with decreasing pressure is consistent with photochemical production at low pressure and downward transport by eddy mixing.

Infrared observations of  $NH_3$  (Tokunaga et al., 1980; Marten et al., 1981; Kunde et al., 1982; Gierasch et al., 1986; Lellouch et al., 1989; Griffith et al., 1992; Carlson et al., 1993, 1994; Encrenaz et al., 1996; Lara et al., 1998) of predominantly the North Equatorial Belt (NEB), the North Tropical Zone (NTZ), the South Tropical Zone (STZ) and the Great Red Spot (GRS) are consistent with theoretical predictions. Near solar or greater abundances of nitrogen, locked in ammonia, at pressures greater than 1 bar have been detected. From 300 to 700 mbar, varying degrees of  $NH_3$  saturation distributions, from about 10 to 100% humidity, are consistent with the observations.

Ultraviolet observations complement those of the infrared. Low spectral resolution ultraviolet observations were demonstrated to be sensitive to higher altitudes where ammonia is depleted by several orders of magnitude by photolysis (Tomasko, 1974). Combes et al. (1981) first identified ultraviolet ammonia features in equatorial spectra of Jupiter, obtained with the IUE, and deduced that the ammonia mixing ratio cannot be constant with altitude. They determined a mixing ratio at 250 mbar in the  $(0.5\text{--}5) \times 10^{-7}$  range. Wagener et al. (1985) used IUE data to determine an ammonia mixing ratio of  $(0.7\text{--}4.3) \times 10^{-8}$  from 100 to 150 mbar and an upper limit of  $1 \times 10^{-9}$  for pressures lower than 100 mbar. Kunde et al.'s (1982) vertical distribution, for pressures greater than 200 mbar, was consistent with their data. Edgington et al. (1998) fitted Hubble Space Telescope (HST) observations of the ultraviolet spectrum of Jupiter at different latitudes by varying the abundance of ammonia at pressures lower than 150 mbar and assuming a saturated ammonia profile from 150 to 670 mbar. Because ammonia is transported from the deep troposphere, the efficiency of vertical transport can be determined in the upper troposphere and complements the acetylene observations.

In this paper, an analysis of the equatorial spectrum of the jovian atmosphere is presented, which includes the effects of rotational and vibrational Raman scattering. This

Table 1  
Viewing geometry

Observation filename	Y15S0401T
Planetographic latitude	0°
Planetographic longitude	270°
Subsolar planetographic latitude	−3.02°
Emission angle	2.4°
Incidence angle	10.4°
Azimuthal angle	75.3°

ultraviolet spectrum was taken with the Faint Object Spectrograph (FOS) on board the HST and exhibits both acetylene and ammonia absorption features. In the next section, the data reduction technique and the Rayleigh–Raman radiative transfer model used in the interpretation of the data are described. Since inclusion of Raman scattering by molecular  $H_2$  in radiative transfer analysis is fairly recent and important to our analysis, Section 3 investigates the effects of various amounts of absorbers on Raman features. Section 4 presents the different atmospheric models that fit the spectrum in terms of acetylene, ammonia, and aerosol vertical distributions. Many aspects of the fit are discussed and compared to previous results. It is shown that acetylene absorption features exist longward of 190.0 nm and that the strength of the features can only be explained by invoking a substantial amount of acetylene below the tropopause. The last section summarizes the results.

## 2. Data reduction and radiative transfer model

The FOS took a 780-s exposure of the jovian equatorial region along the central meridian on June 5, 1993. Table 1 gives the characteristics of the geometry of the observation. The data were obtained through the 1' circular aperture by the G190H grating and red detector combination. The spectrum spans 157.2 to 231.2 nm at a spectral resolution of about 0.3 nm. In this region, the jovian spectrum is determined by the reflective properties of the atmosphere. The data reduction technique has been fully described by Bétrémieux and Yelle (1999) and will only be summarized here.

As the FOS spectrum below 190.0 nm is plagued by scattered light, the baseline of the reflectivity, or I/F, in this region is highly uncertain. The scattered light contribution to the spectrum is assumed to be constant with wavelength and is subtracted from the FOS flat-fielded jovian spectrum. The scattered light contribution was evaluated by determining the average count per unit wavelength below 175.0 nm, not 173.0 nm as was done in Bétrémieux and Yelle (1999). The I/F at 181.5 nm then becomes the same as in the jovian I/F obtained by HUT (Morissey et al., 1995), which is a more reliable instrument than the FOS in that wavelength region.

A theoretical FOS spectrum for a perfectly reflecting Lambertian jovian atmosphere is then computed by

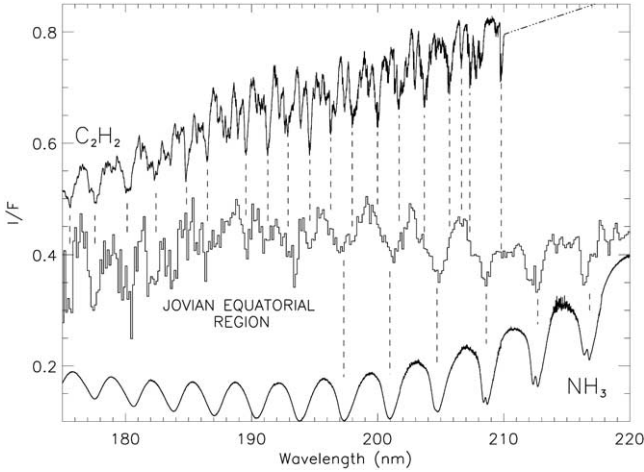


Fig. 1.  $I/F$  of the jovian equatorial region (middle) compared with scaled and offset inverse logarithms of the acetylene (top) and ammonia (bottom) cross sections. The vertical dashed lines identify the more pronounced absorption features in the data. Only the region from 175.0 to 220.0 nm is shown to emphasize the region of molecular absorption.

$$C_{\odot} = \left( \frac{\Omega_{\text{FOS}}}{\pi} \right) \left( \frac{F_{\odot}(1 \text{ AU})}{d^2} \right) S \Delta t, \quad (1)$$

where the solid angle of the FOS,  $\Omega_{\text{FOS}}$ , is  $1.8509 \times 10^{-11}$  sr, Jupiter's heliocentric distance,  $d$ , is 5.4543 AU at the time of the observation,  $\Delta t$  is the exposure time, and  $S$  is the sensitivity of the FOS. The solar flux at the top of the Earth's atmosphere,  $F_{\odot}(1 \text{ AU})$ , was measured by the Solar-Stellar Irradiance Comparison Experiment (SOLSTICE) on March 29, 1992 at a spectral resolution of 0.25 nm.

The scattered-light-corrected FOS spectrum,  $C_{\text{FOS}}$ , and the theoretical spectrum,  $C_{\odot}$ , are then aligned in wavelength using a cross-correlation technique. This first consists in computing the cross-correlation as a function of the wavelength shift of the scattered-light-corrected FOS spectrum with respect to  $C_{\odot}$  over a  $\pm 3$  FOS diode range in increments of  $1/20$  of a diode (or 0.0072 nm). The FOS spectrum is then shifted by the wavelength that maximizes the cross-correlation. The  $I/F$  is finally computed by dividing the resulting shifted FOS spectrum by  $C_{\odot}$ , which has been spectrally degraded to the FOS resolution prior to the division. The latter is done by convolving  $C_{\odot}$  with a gaussian with a full width at half maximum of 0.1743 nm.

Fig. 1 shows the  $I/F$  of the jovian equatorial region binned to one FOS diode or 0.143 nm in the region where ammonia and acetylene absorption are important. Below 175.0 nm, the spectrum is extremely noisy and is not shown. The narrow absorption feature around 193.0 nm is a well-known FOS artifact and should be ignored. Also displayed are scaled and offset inverse logarithm of the cross section of ammonia and acetylene. Displaying the logarithm of the cross section keeps the contrast of the absorption features fairly constant at all wavelengths. The inverse of that should correlate with the  $I/F$  if the constituent is present in the atmosphere. The ammonia cross section was measured be-

low 218.0 nm at a temperature of 175 K by Chen et al. (1999). Above 218.0 nm, measurements from the same authors at 195 K are used but with the local peak of the cross section at 221.2 nm reduced by a factor of 4 to account, albeit in a grossly approximated fashion, for the difference in temperature with the jovian atmosphere. Although the spectrum displays obvious  $\text{NH}_3$  features from 195.0 to 220.0 nm, their shapes are very irregular and do not correspond at all to the smoothness of the  $\text{NH}_3$  cross section. In addition, the correlation with the  $\text{C}_2\text{H}_2$  cross section is striking, and acetylene absorption features can be found at all wavelengths of the spectrum.

Previously detected acetylene absorption features in the jovian planets were almost all located below 190.0 nm. Yelle and McGrath (1996) first showed some evidence for the presence of acetylene features above 190.0 nm in a FOS spectrum of Jupiter obtained at a latitude of  $-48.7^\circ$  just prior to multiple impacts by fragments of the comet Shoemaker-Levy 9. This paper presents the first detailed report of acetylene absorption features above 190.0 nm. Only with the resolution of the FOS is this detection possible. Particularly interesting are the two features around 207.0 nm: the small absorption feature at 206.7 nm and the sharp decrease at 207.2 nm mixed with the ammonia feature. Uncertainties in this region of the spectrum are about 0.3 to 0.4%. The features at 206.7 and 207.2 nm represent variations in the  $I/F$  of 2 and 7% respectively. The signal-to-noise ratio is about 5 and 20, respectively, which confirms that these are not due to statistical noise. The acetylene cross section was measured up to 210.0 nm at a spectral resolution of 0.007 nm and a temperature of 155 K (Chen et al., 1991). Because acetylene absorption is still important up to 210.0 nm, it seems likely to be so at longer wavelengths where no acetylene cross-section data are currently available. For the analysis presented in this paper, the logarithm of the  $\text{C}_2\text{H}_2$  cross section is extrapolated linearly to longer wavelengths. Above 210.0 nm, the equatorial spectrum displays molecular hydrogen ( $\text{H}_2$ ) Raman features. These features have already been identified and dealt with at length for this particular spectrum by Bétrémieux and Yelle (1999; see their Fig. 12).

The cross section of  $\text{H}_2$  decreases with increasing wavelength: Longer wavelength photons can reach deeper regions of the jovian atmosphere. Fig. 2 shows the pressure for which the optical depth reaches unity for a clear jovian atmosphere. The atmosphere consists of a mixture of 86.5%  $\text{H}_2$  and 13.5% He as measured by the Galileo probe (Niemann et al., 1996, 1998). The calculations shown in Fig. 2 are for this FOS observation's specific incidence angle. For a conservative atmosphere, photons can propagate to roughly twice the depth indicated in Fig. 2. The detection of  $\text{C}_2\text{H}_2$  features above 190.0 nm allows determination of the acetylene distribution to deeper levels in the jovian atmosphere than had previously been possible. The dashed lines bracket the wavelength region where the longest-wavelength identified acetylene features are located. Whereas

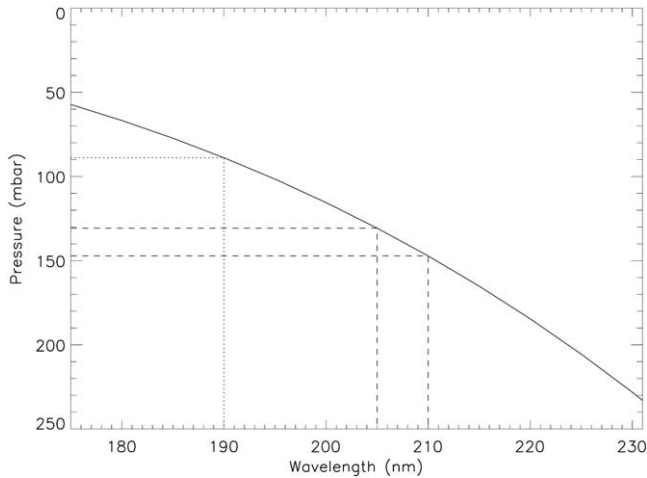


Fig. 2. Pressure level where the  $\text{H}_2$  optical depth reaches unity as a function of wavelength for a clear jovian atmosphere and a solar zenith angle of  $10.4^\circ$ . The dashed lines bracket the wavelength region where the acetylene features of interest are located. The dotted line defines the pressure region probed by 190.0-nm photons.

features below 190.0 nm probe mostly above the 90-mbar level in the stratosphere, the long-wavelength features can probe below the 130-mbar level in the upper troposphere.

To interpret the equatorial I/F, the Rayleigh–Raman radiative transfer model described by Bétrémieux and Yelle (1999) is used. As Raman scattering by molecular hydrogen shifts photons by at least several FOS resolution elements, it cannot be ignored in the modeling of the reflectivity. The background atmospheric model, to which minor gaseous species and aerosols will be added, consists of the same  $\text{He}/\text{H}_2$  ratio that the Galileo probe found. The ortho/para ratio of molecular hydrogen is prescribed by an equilibrium population at 130 K. The use of an equilibrium  $\text{H}_2$  population over a normal one does not significantly affect the I/F at jovian atmospheric temperatures, as was demonstrated previously (Bétrémieux and Yelle, 1999). The gravitational acceleration is taken to be constant throughout the atmosphere and is evaluated at the 100-mbar level. Using the gravity harmonics determined by Pioneer 11 (Anderson, 1976), the gravitational acceleration is found to be  $2311 \text{ cm s}^{-2}$  at the equator. The bottom boundary of the atmosphere is treated as a perfectly reflecting Lambertian surface, consistent with the presence of a highly reflective and optically thick cloud. This background atmosphere will be referred to as a clear jovian atmosphere throughout this paper.

The atmosphere is divided into different pressure regions where the properties of existing gaseous absorbers, clouds, and aerosols can be specified. Gaseous absorbers are characterized by their mole fraction,  $f$ , and their wavelength-dependent absorption cross sections,  $\sigma(\lambda)$ . Since polyacetylenes, which probably make up the stratospheric haze, are spherical (Bar-Nun et al., 1988), their optical properties can be computed using Mie scattering theory. The inputs consist of the real and imaginary indices of refraction,  $n_{\text{R}}$  and  $n_{\text{I}}$ , as well as the distribution of particle radii. The distribution

function is a log-normal distribution specified by the mean,  $r_{\text{aero}}$ , and the variance,  $\sigma_{\text{aero}}$ , of the particle radius. The column number density of aerosols is also specified for each layer. Ammonia ice particulates, by contrast, are nonspherical (Pope et al., 1992) and cannot be treated by Mie scattering. Ammonia clouds are then characterized by their single-scattering albedo  $\omega_{\text{cl}}$ , their extinction optical depth  $\tau_{\text{cl}}$ , and their scattering phase functions  $P_{\text{cl}}$ . The latter is a double Henyey–Greenstein phase function described by a forward,  $g_{\text{f}}$ , and backward,  $g_{\text{b}}$ , asymmetry factor as well as the fraction,  $f_{\text{cl}}$ , of light that scatters forward.

The I/F is computed every 0.1 nm via a discrete ordinates method using 10 layers spanning pressures from 0 to 700 mbar and 32 streams. Ten layers are sufficient to model the I/F accurately. The changes in the I/F caused by doubling the number of layers are well below the uncertainty of the data. To compare the I/F produced by the radiative transfer model to the I/F obtained by the FOS, a theoretical count rate is computed from the modeled I/F. The resulting spectrum is then degraded to the spectral resolution of the FOS in the same way as  $C_{\odot}$  had been when computing the I/F of Jupiter, before it is finally divided by  $C_{\odot}$ . To fit the jovian spectrum, the acetylene and ammonia vertical distributions are first determined based on the amplitude of the absorption features. Aerosols or clouds must then be added to modify the continuum level. Since these will partly or entirely hide the atmosphere beneath, the gaseous constituents' vertical profile must then be readjusted to preserve the depth of the absorption features, and so on. The moderate resolution of the data combined with its high signal-to-noise ratio make this technique particularly challenging, as many iterations are required before an acceptable fit is reached. One new dimension in this procedure is the fitting of the Raman features. Although their shapes are dependent on the ortho/para ratio of molecular hydrogen, their amplitudes are mostly dependent on the abundance and optical properties of absorbers and scatterers present in the atmosphere, which provides new constraints on atmospheric models.

### 3. Raman constraint on tropospheric clouds

The slow decrease of the I/F longward of 220.0 nm is generally attributed to the presence of dark clouds in the troposphere. To explain the I/F above 220.0 nm of a jovian equatorial spectrum obtained by IUE, Wagener et al. (1985) used 1.5 optical depths of clouds with a single-scattering albedo of 0.42 from 150 to 600 mbar. However, because the effects of Raman scattering by  $\text{H}_2$  were ignored, the modeled I/F is featureless above 220.0 nm and the abundance of clouds and aerosols are poorly constrained. Inclusion of Raman scattering changes the results of radiative transfer calculations for the jovian atmosphere significantly. Instead of treating molecular hydrogen as a partial absorber, it is now treated as a pure scatterer, and ultraviolet photons can propagate deeper than previously thought. The amplitude of

Table 2  
Absorber/scatterer characteristics for Raman investigation

Model	$\omega$	$\tau$	Pressure (mbar)
a	0.00	0.3	20–60
b	0.75	1.2	20–60
c	0.00	0.3	120–160
d	0.00	0.3	220–260
e	0.00	0.4	220–260
f	0.75	1.2	220–260
g	0.00	0.3	420–460
h	0.00	3.0	420–460

features produced by partial filling of solar absorption lines are sensitive to the presence of clouds, aerosols, and gaseous absorbers. These Raman features provide a means to ascertain the aerosol and cloud content of an atmosphere from regions of the spectrum which were previously modeled as featureless regions, and the model of Wagener et al. (1985) can be reevaluated.

To understand the effect of absorbers and scatterers on Raman features, the results of a few simple models are presented and compared to the equatorial I/F. Table 2 shows the different models used for this purpose, each of which is identified with a letter that will be used throughout this section. The single-scattering albedo,  $\omega$ , extinction optical depth,  $\tau$ , and location in pressure of the different absorbers and scatterers are specified. Obviously, pure absorbers are represented by nil single-scattering albedos while the others are scatterers. The single-scattering albedo and extinction optical depth are all wavelength independent. The absorbers and scatterers are embedded in 1.1 bar of a clear jovian atmosphere.

Fig. 3 compares the model I/F of different distributions of pure absorbers in the jovian atmosphere to the equatorial

I/F. In Fig. 3a, 0.3 optical depth of pure absorbers are placed at different depths. Absorbers located higher in the atmosphere (lower pressure regions), produce a lower I/F. However, the dependence of the amplitude of the Raman features on the location of the absorbers is more complex. From model g, to d and c, as the absorbers are displaced to lower pressures, the I/F decreases and so do the Raman features. However as the absorbers are pushed even higher, in the upper stratosphere as in model a, the trend reverses and although the I/F still diminishes, the Raman features now increase. This can only be explained when the contribution to the I/F from multiple Raman scattering is important. Kaminski and McConnell (1991) showed that in a nearly conservative and optically thick atmosphere, enhancement of up to a factor of 5 in the average specific intensity could be achieved compared to an optically thin atmosphere with a purely absorbing lower boundary. Although nothing as dramatic is expected in the jovian atmosphere because of the presence of pure absorbers, multiple scattering should still be fairly important. When absorbers are located at low pressures, they do not impede multiple scattering deep in the atmosphere. So, although fewer photons escape the atmosphere, a higher fraction of them have actually Raman scattered; hence the features are bigger relative to the I/F continuum. As absorbers are located deeper in the atmosphere, multiple Raman scattering is short-circuited and smaller fractions of the escaping photons have Raman scattered. Hence, the amplitude of Raman features are biggest relative to the I/F baseline when the absorber is highest in the atmosphere.

Fig. 3b shows the effect of increasing the abundance of pure absorbers at pressures higher than 200 mbar. As expected, the presence of more absorbers reduces not only the I/F but the size of the Raman features as well, since the

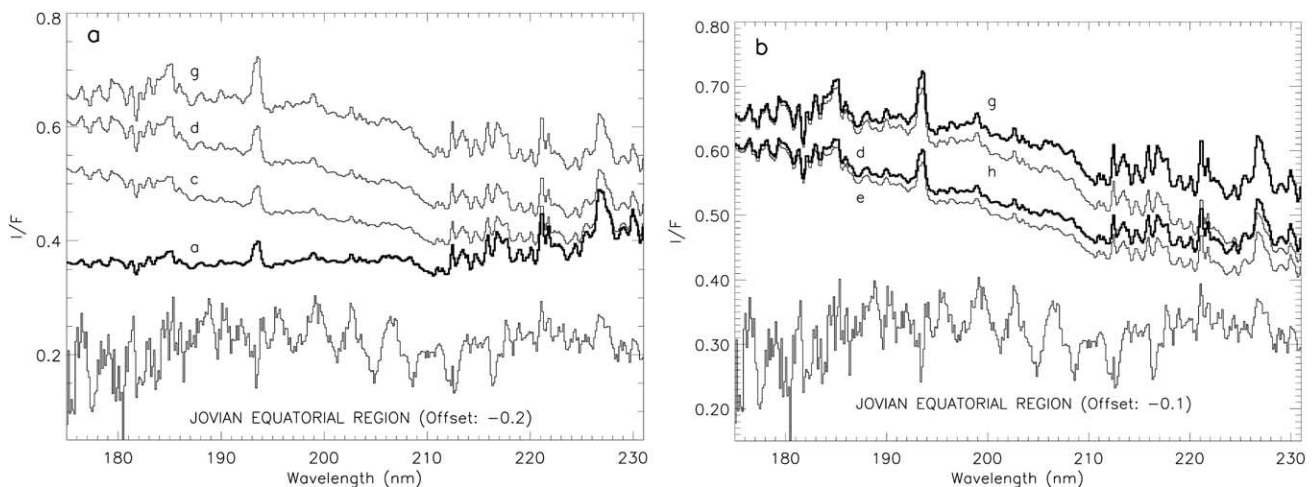


Fig. 3. Comparison of the data with different model I/F. The abundance and location of pure absorbers are varied in 1.1 bar of clear jovian atmosphere with a bottom surface albedo of 1.00. Each curve is associated with a letter indexed to Table 2. (a) The location of 0.3 optical depth of pure absorber is varied. The amplitude of the Raman features are biggest relative to the I/F baseline when the absorber is highest in the atmosphere (thick line). (b) The optical depth of the absorber is varied in two different pressure regions. The Raman features decrease as the absorbers' abundance increases at a given pressure level.

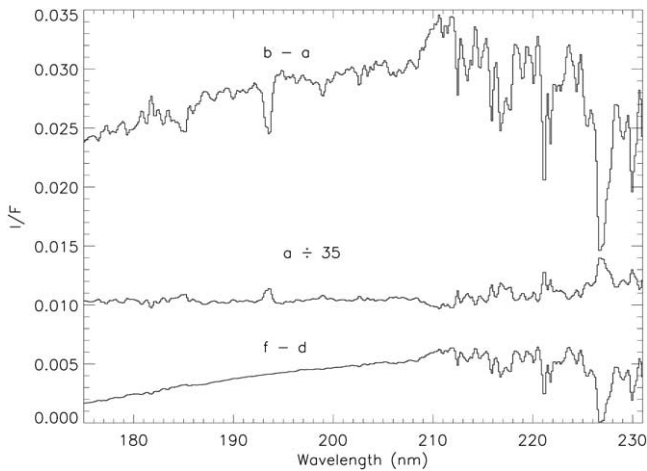


Fig. 4. Difference in model I/F between one with scatterers and one with absorbers. The scatterers and absorbers have identical absorption optical depth and are described in Table 2. Also shown for comparison is the scaled result of model a. As expected, the scatterer increases the I/F, but the clear anticorrelation between the scaled model and the model difference means that the size of the Raman features have also decreased. The presence of scatterers decreases the relative size of Raman features with respect to the I/F continuum.

probability for a photon to undergo a Raman transition per collision decreases. Most of the models contain smaller Raman features above 210.0 nm than are present in the data. Although model g has Raman features comparable to the equatorial spectrum, its I/F is much higher. To reduce the I/F, more absorbers are needed. However, even a factor 10 increase in the absorbers' abundance below 400 mbar, exemplified in model h, is not enough to reduce the I/F to the level of the data, but the Raman features are now significantly smaller. Only model a produces strong Raman features for a low I/F, when the absorbers are located in the upper stratosphere, not in the troposphere.

How do the sizes of Raman features change if the absorbing particles are also scatterers? To investigate this question, the I/F produced by models a and d are compared to those produced by b and f. The extinction optical depth and single-scattering albedo of the scatterers are chosen so that the absorption optical depth is identical to those of the pure absorbers. The scattering phase function is described by a double Henyey–Greenstein phase function with  $g_f = 0.80$ ,  $g_b = -0.80$ , and  $f_{cl} = 0.969$ , which was inferred by Tomasko et al. (1978; see their Table 4) from Pioneer 10 observations. Fig. 4 shows the difference in I/F for models with scatterers and pure absorbers and compares it to a scaled version of model a. Although less pronounced for the deeper lying species, scatterers increase the I/F. However, judging from the anticorrelation between the differences and the scaled model, scatterers decrease the relative amplitude of the Raman features with respect to the I/F continuum. Hence, the choice of scatterers over absorbers does not help in explaining the high amplitude of the Raman features combined with the low I/F of the data.

It is clear that no optically significant amount of dark clouds, aerosols, or gaseous absorbers can be located from 100 to 500 mbar, contrary to Wagener et al.'s (1985) model. This is demonstrated by comparing the I/F obtained by using the cloud and aerosols best-fit model of Wagener et al. (1985) to the equatorial I/F. The model consists of 600 mbar of clear jovian atmosphere, free of gaseous absorbers, with a lower boundary described by a perfectly reflecting Lambertian. Clouds, with a wavelength-independent single-scattering albedo of 0.42 and an optical depth of 1.5 are located between 150 to 600 mbar. Their phase function is described by a double Henyey–Greenstein phase function with the following parameters:  $g_f = 0.80$ ,  $g_b = -0.65$ , and  $f_{cl} = 0.95$ . The top haze layer is located at 50 mbar with a column abundance of  $4.96 \times 10^7 \text{ cm}^{-2}$ . It is composed of particles whose size distribution is parameterized by a log-normal distribution with a mean radius of  $0.4 \mu\text{m}$  and a variance of 0.05. Combined with an index of refraction  $n = 1.4 + 0.0015i$ , the characteristics of this haze reproduce the optical properties of the haze used by Wagener et al. (1985). As shown in Fig. 5, the resulting Raman features are about half as big as those in the data. Since dark tropospheric clouds cannot explain the reflective properties above 220.0 nm, the solution must be sought in the optical properties of stratospheric gaseous absorbers or aerosols.

Wagener et al. (1985) could not determine the clouds' location from their ultraviolet data because they did not include Raman scattering in their analysis. Instead, Wagener et al. (1985) relied on previous determination of the clouds' location obtained from visible spectra. However, analysis of visible spectra are dependent on the accuracy of methane absorption coefficients, which, for the cold temperatures of the jovian atmospheres, have only been measured in small wavelength intervals (Smith et al., 1990; Larson and Mickelson, 1993). Infrared spectra have also

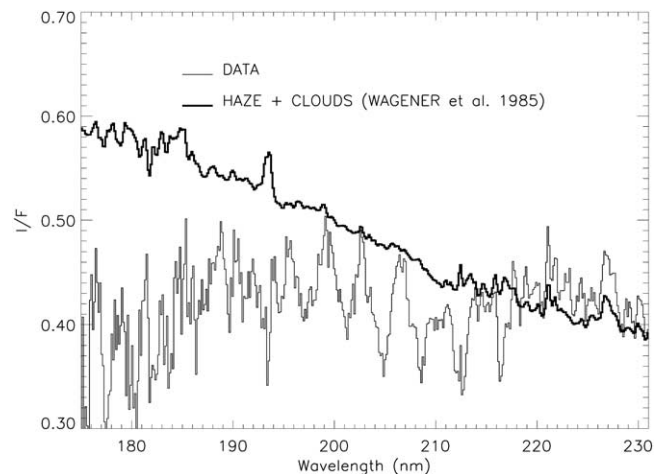


Fig. 5. Comparison of the data with the model I/F of a clear jovian atmosphere free of molecular absorbers with the same haze and cloud content as Wagener et al. (1985). See text for a more detailed description. The amplitudes of the modeled Raman features are too small by at least a factor of 2.

Table 3  
C<sub>2</sub>H<sub>2</sub> distribution

Pressure (mbar)	Mole fraction						
	A	B, C	D, J	E	F	G	H
0–20	$4 \times 10^{-8}$	$4 \times 10^{-8}$	$4 \times 10^{-8}$	$2 \times 10^{-8}$	$5 \times 10^{-8}$	$4 \times 10^{-8}$	$4 \times 10^{-8}$
20–60	$1.5 \times 10^{-8}$ <sup>a</sup>	$1.5 \times 10^{-8}$ <sup>a</sup>	$1.5 \times 10^{-8}$ <sup>a</sup>	$3 \times 10^{-8}$ <sup>a</sup>	$1 \times 10^{-8}$ <sup>a</sup>	$1 \times 10^{-8}$ <sup>a</sup>	$1.5 \times 10^{-8}$ <sup>a</sup>
60–80	$5 \times 10^{-9}$ <sup>a</sup>	$5 \times 10^{-9}$	$4 \times 10^{-8}$	$4 \times 10^{-8}$	$4 \times 10^{-8}$	$4 \times 10^{-8}$	$4 \times 10^{-8}$
80–100	$5 \times 10^{-9}$ <sup>a</sup>	$1.5 \times 10^{-7}$	$8 \times 10^{-8}$	$8 \times 10^{-8}$	$8 \times 10^{-8}$	$1.2 \times 10^{-7}$	$8 \times 10^{-8}$
100–120	$5 \times 10^{-9}$	$1.5 \times 10^{-7}$	$8 \times 10^{-8}$	$8 \times 10^{-8}$	$8 \times 10^{-8}$	$1.2 \times 10^{-7}$	$8 \times 10^{-8}$
120–150	$1 \times 10^{-7}$	$1.5 \times 10^{-7}$	$1.5 \times 10^{-7}$	$1.5 \times 10^{-7}$	$1.5 \times 10^{-7}$	$1.2 \times 10^{-7}$	$1.5 \times 10^{-7}$
150–200	$5 \times 10^{-7}$	$1.5 \times 10^{-7}$	$1.5 \times 10^{-7}$	$1.5 \times 10^{-7}$	$1.5 \times 10^{-7}$	$1.2 \times 10^{-7}$	$2 \times 10^{-7}$
200–300	$2 \times 10^{-7}$	$1.5 \times 10^{-7}$	$1.5 \times 10^{-7}$	$1.5 \times 10^{-7}$	$1.5 \times 10^{-7}$	$1.2 \times 10^{-7}$	$2 \times 10^{-7}$
300–700		$1.5 \times 10^{-7}$	$1.5 \times 10^{-7}$	$1.5 \times 10^{-7}$	$1.5 \times 10^{-7}$	$1.2 \times 10^{-7}$	$2 \times 10^{-7}$
700–1100				(I) $1.5 \times 10^{-7}$			

<sup>a</sup> Aerosols present.

been used to infer the presence of upper tropospheric clouds. However, these are sensitive to the temperature profile of the jovian atmosphere. Reliable temperature measurements of the upper troposphere and above are very sparse, existing only for the Equatorial Zone (EZ) and the South Equatorial Belt (SEB) from Voyager 1 occultation data (Lindal et al., 1981) and more recently for the NEB by the Galileo probe (Seiff et al., 1996, 1998). In other regions the temperature profile must be deduced from analysis of infrared data; typically a profile is found by perturbing the Voyager 1 profile around the tropopause and in the lower stratosphere. Analysis of Raman features in ultraviolet spectra present the advantage of constraining both gaseous absorbers and aerosols simultaneously and self-consistently.

#### 4. Interpretation of spectrum and discussion

The size of absorption features depends to first order on the column abundance modulated by the atmospheric depth of the responsible species. The important species absorb over a broad wavelength range and changing the mole fraction of a species in one pressure range can affect most of the spectrum. Conversely, a host of different altitude distributions can explain a single spectral feature. The most

probable distribution can be inferred only by looking at the entire spectrum. Since the I/F at one wavelength is correlated with the I/F at another wavelength, uncertainties on the altitude distribution are even more difficult to quantify. Rather than estimate the uncertainty on the abundance of a molecular species for each pressure region, different distributions that all closely fit the data will be presented; these should provide some idea as to what the uncertainties are. Several combinations of aerosol, acetylene, and ammonia distributions provide an excellent fit to the FOS spectrum over the 175.0- to 232.0-nm region. The distribution of acetylene and location of aerosols are described in Table 3, while the ammonia distribution is given by Table 4. The optical properties of the aerosols are specified by Table 5. The different models, identified with capital letters, produce I/F's that are identical to each other to within 0.01 above 196.0 nm, and 0.02 below. All models consist of 700 mbar of a clear jovian atmosphere except for model I, which extends down to 1.1 bar. From these models, model D produces the best fit to the spectrum and is shown in Fig. 6.

As mentioned previously, the relatively high strength of the Raman features combined with a low reflectivity excludes the presence of optically significant amounts of tropospheric clouds or gaseous absorbers. Only with a perfectly reflecting optically thick cloud at 700 mbar, combined with a fairly absorbing stratospheric haze, could

Table 4  
NH<sub>3</sub> distribution

Pressure (mbar)	Mole fraction			
	A	B	C–I	J
0–60	—	—	—	—
60–80	$3 \times 10^{-10}$	—	—	—
80–100	$3 \times 10^{-10}$	$1.2 \times 10^{-9}$	$1 \times 10^{-9}$	$5 \times 10^{-10}$
100–120	$1.5 \times 10^{-9}$	$1.2 \times 10^{-9}$	$1 \times 10^{-9}$	$5 \times 10^{-10}$
120–150	$1.5 \times 10^{-9}$	$1.5 \times 10^{-9}$	$2 \times 10^{-9}$	$3 \times 10^{-9}$
150–200	$2 \times 10^{-9}$	$2.5 \times 10^{-9}$	$3 \times 10^{-9}$	$3 \times 10^{-9}$
200–300	$3 \times 10^{-9}$	$3.5 \times 10^{-9}$	$4 \times 10^{-9}$	$4 \times 10^{-9}$
300–400	$5 \times 10^{-9}$	$4 \times 10^{-9}$	$5 \times 10^{-9}$	$5 \times 10^{-9}$
400–700	$1 \times 10^{-8}$	$5 \times 10^{-9}$	$5 \times 10^{-9}$	$5 \times 10^{-9}$

Table 5  
Haze imaginary index of refraction

Wavelength (nm)	A–G, J	H	I
120.0	0.0001	0.0001	0.0001
200.0	0.0001	0.0001	0.0001
203.0	0.0025	0.0025	0.0025
204.0	0.0030	0.0030	0.0030
215.0	0.0120	0.0110	0.0110
222.0	0.0180	0.0180	0.0140
224.0	0.0200	0.0200	0.0160
228.0	0.0280	0.0280	0.0230
235.0	0.0280	0.0280	0.0230

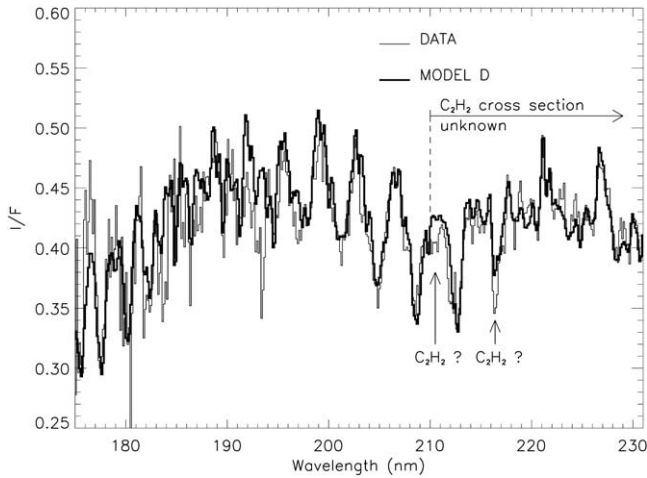


Fig. 6. Comparison of the data with the I/F produced by model D. The acetylene features around 207.0 nm are well matched. Differences from 211.0 nm to 217.0 nm are due to the inadequacies of the  $C_2H_2$  cross section above 210.0 nm. The absorption feature at 216.1 nm is too narrow to be caused by ammonia and might be due to acetylene since acetylene absorption bands are found throughout the FOS spectrum of Jupiter where the ultraviolet absorption cross section of acetylene is known.

the Raman features be matched. The location of the bottom reflecting cloud is consistent with theoretical predictions of the location of the  $NH_3$  cloud deck. Model I showed that the location of the bottom cloud could be pushed down to 1.1 bar, provided the stratospheric haze's optical properties were adjusted, but not any further. The size of the Raman features decreases as the cloud is located deeper, and at 1.1 bar, the feature at 221.0 nm is already smaller than its counterpart in the equatorial spectrum.

The ammonia vertical profile can be deduced from the interpretation of prominent ammonia absorption features from 195 to 218 nm in Jupiter's spectrum. However, the relative depth of the ammonia features at 201.0 and 205.0 nm could not be explained with any combinations of  $NH_3$  or  $C_2H_2$  profiles. Featureless absorbers such as  $H_2S$  and  $OCS$  were considered but did not yield a better fit. Attempts with haze and clouds with imaginary indices of refraction independent of wavelength were unsuccessful as well, as the I/F slope would be too shallow. Only a sudden increase with wavelength around 201.0 nm by a factor of 25 in the imaginary index of refraction of the stratospheric haze could fit the data. The properties of the haze are otherwise left largely unconstrained by the data. To fit the spectrum, only the imaginary index of refraction is left as a free parameter; everything else is set. The stratospheric haze's real index of refraction is 1.4. The size distribution of the particles is defined by a log-normal distribution with a mean of  $0.3 \mu m$  and a variance of 0.05. A column abundance of  $2 \times 10^8 \text{ cm}^{-2}$  homogeneously mixed from 20 to 60 mbar is used in all models, except for model A where the haze extends from 20 to 100 mbar. Table 5 shows the resulting imaginary index of refraction of the haze for different wavelengths. At intermediate wavelengths, the index is defined by linear

interpolation between the defined values. The optical properties of the haze determines the I/F continuum above 210.0 nm.

Above 210.0 nm, simultaneous ignorance of the acetylene cross section and the optical properties of the stratospheric haze makes the interpretation of the spectrum hazardous. Only parts of the spectrum, where either the haze or the acetylene's optical properties, but not both, determine the behavior of the I/F can be used reliably to infer the haze's optical properties and the acetylene's vertical distribution. Hence, the abundance of tropospheric acetylene is determined predominantly from the acetylene features located between 200 and 210 nm, where the aerosols' properties do not impact significantly the I/F. Above 217.0 nm, as demonstrated in the previous sections, the I/F is mainly determined by the optical properties of materials in the stratosphere. As a result, the imaginary index of refraction can be determined with some confidence, given the assumptions made about the distribution of the haze particles, and the fit to the data is reasonable. Between 210.0 and 217.0 nm, both acetylene and stratospheric haze contribute significantly to the spectrum. The model I/F in this spectral region is substantially above the spectra. Because it is impossible to determine whether the haze properties or the assumed acetylene cross section needs to be modified, a better fit to the spectrum was not attempted. Fig. 7 clearly demonstrates that the stratospheric haze is necessary to fit the continuum. This haze is highly reflective below 203.0 nm and becomes more absorbent with increasing wavelength. Previous determination of the jovian stratospheric haze's optical properties in the ultraviolet by Tomasko et al. (1986) yielded the opposite behavior above 221.0 nm, which agreed well with laboratory determination of the optical properties of candidate aerosols (Noy et al., 1979; Bar-Nun et al., 1988). However, dark clouds from 300 to 700 mbar were used to

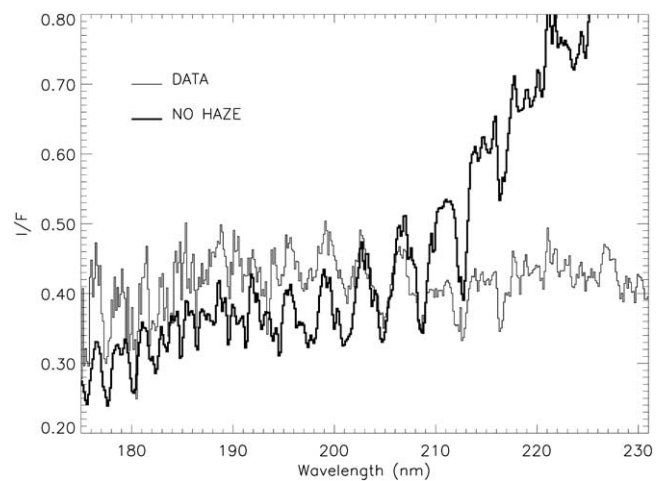


Fig. 7. Comparison of the data with the I/F resulting from model D where the stratospheric haze has been removed. The absence of the stratospheric haze causes the long-wavelength spectrum to be extremely bright and the short-wavelength spectrum to be too dark.

Table 6  
Model with tropospheric clouds

Pressure (mbar)	Mole fraction		Cloud optical depth	Haze properties	
	C <sub>2</sub> H <sub>2</sub>	NH <sub>3</sub>		Wavelength (nm)	<i>n</i> <sub>1</sub>
0–20	4 × 10 <sup>−8</sup>	—	—	140	0.0012
20–60	2.5 × 10 <sup>−8</sup>	—	<sup>a</sup>	180	0.0018
60–80	1.5 × 10 <sup>−8</sup>	—	—	200	0.0030
80–120	1.5 × 10 <sup>−8</sup>	1 × 10 <sup>−9</sup>	—	203	0.0040
120–150	1.5 × 10 <sup>−8</sup>	2 × 10 <sup>−9</sup>	—	204	0.0050
150–200	1.5 × 10 <sup>−8</sup>	3 × 10 <sup>−9</sup>	0.64	215	0.0130
200–300	—	1 × 10 <sup>−8</sup>	1.60	222	0.0190
300–400	—	1 × 10 <sup>−7</sup>	2.00	224	0.0210
400–550	—	1 × 10 <sup>−6</sup>	4.00	228	0.0300
550–700	—	1 × 10 <sup>−5</sup>	20.0	235	0.0290

<sup>a</sup> Aerosols present.

explain the decrease of the I/F with increasing wavelength, rather than by stratospheric haze alone, and these were shown in the previous section to be inconsistent with the amplitude of the Raman features seen in the FOS spectrum.

The large amplitude of ammonia features is also a challenge to reproduce. As shown in Table 4, only small quantities of NH<sub>3</sub>, well below its saturation point at these pressures, can fit the data. Presumably, below the cloud deck, located here at 700 mbar, the NH<sub>3</sub> mole fraction can increase quickly with pressure and reach values consistent with past infrared observations since the spectrum is not sensitive to constituents located this deep. The NH<sub>3</sub> distribution is reminiscent of Bjoraker et al.'s (1986) H<sub>2</sub>O vertical profile from 2 to 4 bars, which was subsequently explained by Lunine and Hunten (1987) in terms of narrow moist convective plumes. This NH<sub>3</sub> distribution is irreconcilable with previously reported abundances of NH<sub>3</sub> in the troposphere of Jupiter (Tokunaga et al., 1980; Combes et al., 1981; Kunde et al., 1982; Wagener et al., 1985; Lara et al., 1998; Edgington et al., 1998), which are orders of magnitude higher below 200 mbar. Fig. 8a shows the I/F produced by a mole fraction of 2 × 10<sup>−7</sup> of NH<sub>3</sub> from 200 to 600 mbar, the bottom of which is perfectly reflecting. The model NH<sub>3</sub> bands do not resemble those from the data at all. Adding haze in the stratosphere does not help either. Using the same stratospheric haze as in Fig. 5 with a column abundance of 2 × 10<sup>7</sup> cm<sup>−2</sup> decreases the NH<sub>3</sub> absorption features' size. Clouds could be added in the troposphere to shield the bulk of the ammonia. However, to avoid decreasing the Raman features too much, the clouds must be perfectly reflective. Table 6 describes a model that best fits the ammonia absorption features in the equatorial spectrum when tropospheric clouds are included from 150 to 700 mbar with a tropospheric ammonia distribution slightly depleted compared to Lara et al.'s (1998) 10° south model. The aerosols from 20 to 60 mbar have the same size distribution, column abundance, and real index of refraction as those in model D. Their imaginary index of refraction is listed as a function of wavelength in Table 6. The tropospheric clouds' phase function is that of Wagener et al.

(1985), also used in the model that produced Fig. 5. The cloud particles' single-scattering albedo is set to 1. Fig. 8b compares the resulting model I/F to the equatorial spectrum. Although the depth of the NH<sub>3</sub> features are well matched, the Raman features from 215.0 to 225.0 nm are substantially reduced by NH<sub>3</sub> absorption and do not fit the data.

The discrepancy of the derived NH<sub>3</sub> distribution with previous measurements is of some concern. Clearly, NH<sub>3</sub> and cloud distributions that are consistent with condensation of ammonia between 150 and 700 mbar cannot explain the equatorial spectrum because the Raman features longward of 215.0 nm become too shallow. The results of Combes et al. (1981), Wagener et al. (1985), and Edgington et al. (1998) were consistent with NH<sub>3</sub> clouds in this region only because the effects of H<sub>2</sub> Raman scattering on ultraviolet spectra were ignored. Infrared spectra, which are sensitive to deeper regions of the atmosphere, also agree with their conclusions. However, in addition to the issues with temperature uncertainties mentioned in the previous section, many caveats exist in past analyses of infrared spectra. IRIS spectra suffer from low signal-to-noise ratios. Marten et al. (1981), Kunde et al. (1982), Gierasch et al. (1986), Griffith et al. (1992), and Carlson et al. (1993, 1994) averaged together many spectra, over all longitudes within small latitudinal bands and from 0 to 30° in emission angles, to improve the signal-to-noise. More recent observations looked at a larger fraction of the jovian atmosphere simultaneously. The observations of Lara et al. (1998) and Fouchet et al. (2000) covered a latitudinal range of 10–36° South and ±30° respectively. Furthermore, Fouchet et al. (2000) observed Jupiter for 110 min during which time Jupiter rotated about a fifth of its circumference or 72° in longitude. This contrasts markedly with the 3° latitudinal and longitudinal extent of the FOS observation presented in this paper. Since the relationship between the flux level at a given wavelength and the abundance of a given constituent is nonlinear, it is unclear that the inferred vertical distributions of gas and aerosols represent an average state of the jovian atmosphere. Furthermore, these analyses, as well as those of Tokunaga et al. (1980), only explore small varia-

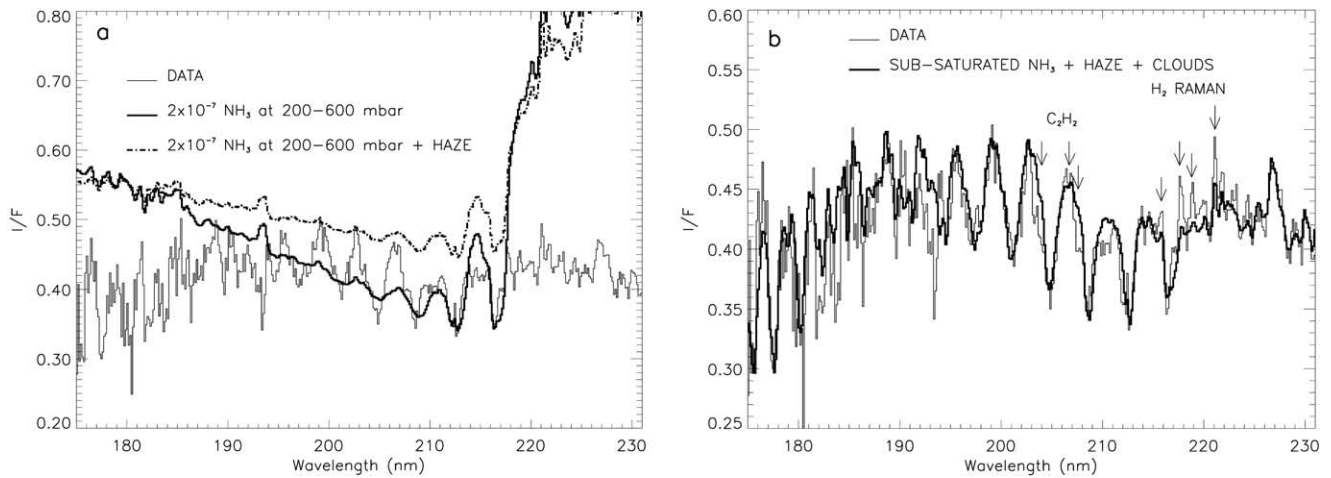


Fig. 8. Comparison of data with models having ammonia abundances in the troposphere consistent with past observations. (a) 600 mbar of clear jovian atmosphere with a perfectly reflecting bottom boundary is used. Both models have an  $\text{NH}_3$  mole fraction of  $2 \times 10^{-7}$  from 200 to 600 mbar. The haze in one of the models is the same stratospheric haze as used in Fig. 5 but with a column abundance of  $2 \times 10^7 \text{ cm}^{-2}$ . The ammonia features are obviously saturated and do not match the data at all. The effect of the haze is only to increase the baseline I/F and decrease the features. (b) The model listed in Table 6 is used. The aerosols are the same as in model D and the tropospheric clouds have a single scattering albedo of 1 and a scattering phase function identical to Wagener et al.'s (1985) tropospheric haze. Although the  $\text{NH}_3$  features match the data, the  $\text{H}_2$  Raman features indicated by the arrows are much too small. The acetylene ( $\text{C}_2\text{H}_2$ ) features are also too weak or even nonexistent compared to the observed spectrum.

tions of vertical  $\text{NH}_3$  distribution, all of which are consistent with subsaturation by a factor of several, followed by a sudden decrease at higher altitudes due to photolysis. The  $\text{NH}_3$  distribution inferred from the FOS spectrum, displayed in Table 4, is fairly constant in altitude and extends in significant quantities at pressures below 200 mbar, regions to which ultraviolet spectra are very sensitive. This kind of extended  $\text{NH}_3$  distribution has not been previously considered in past analyses of infrared spectra. Unfortunately, the Galileo probe (Niemann et al., 1998) only determined an upper limit of  $2 \times 10^{-3}$  for ammonia at pressures greater than 15 bar and cannot resolve the discrepancies between ultraviolet and infrared measurements.

It is also possible that the  $\text{NH}_3$  distribution is inaccurate because the  $\text{NH}_3$  ultraviolet cross section used was, in fact, measured at a temperature of 175 K, substantially warmer than the upper troposphere, which ranges from 110 to 140 K. Dick and Ziko (1973) confirmed through laboratory measurements that ammonia absorption longward of 216.7 nm comes from vibrationally excited states. Absorption due to these “hot bands” should decrease substantially with temperature. Dick and Ziko (1973) computed that the absorption cross section at 221.2 nm should decrease by factors of 145 and 2133 when the temperature decreases from 295 K to 140 and 110 K respectively. Since the inferred lack of  $\text{NH}_3$  in this paper relies on the size of Raman features above 217.0 nm, where absorption from  $\text{NH}_3$  is due exclusively to these “hot bands,” the ammonia distribution that can accommodate the FOS spectra depends critically on the temperature at which the cross section of  $\text{NH}_3$  has been measured. As a result, the abundance of ammonia for pressures greater than 200 mbar is highly uncertain and could possibly agree with infrared measurements. High-resolution

measurements of the ultraviolet ammonia cross section at the temperatures of the outer planets' upper tropospheres are needed to interpret ultraviolet data accurately.

Although model D fits the Raman features well, the ammonia feature produced by the model at 216.1 nm is much shallower than the data. However, looking at that  $\text{NH}_3$  feature in the data with more care, it seems that two components exist: one shallow and broad feature, whose width is matched by the model-produced ammonia feature, and one very narrow feature offset from the core of the absorption. It is likely that this feature is not caused by  $\text{NH}_3$  but by some other absorber, possibly  $\text{C}_2\text{H}_2$  (see Fig. 6) since its cross section is unknown at these wavelengths.<sup>2</sup> It is also possible that the optical properties attributed to the stratospheric haze are actually the combined effect of a highly reflective haze layer and some unknown gaseous absorber or absorbers whose cross section peaks above or around 230.0 nm. This absorber might also be responsible for the narrow absorption at 216.1 nm. Smith et al. (1998) recently measured the absorption cross section of diacetylene ( $\text{C}_4\text{H}_2$ ) at a temperature of 193 K from 195.0 to 265.0 nm and found that the cross section is highly structured and presents many narrow peaks. These may not be at the right wavelengths to explain the equatorial spectrum, but the fact that a fairly simple hydrocarbon that may be present in Jupiter's atmosphere can absorb at these long wavelengths suggests that it may not be the only one. Clearly, more high-resolution laboratory measurements of hydrocarbons at these longer

<sup>2</sup> Since this paper was first submitted, this hypothesis was confirmed by Bénilan et al. (2000). Their measurements of the acetylene ultraviolet cross section indeed show that acetylene has an absorption band at 216.1 nm.

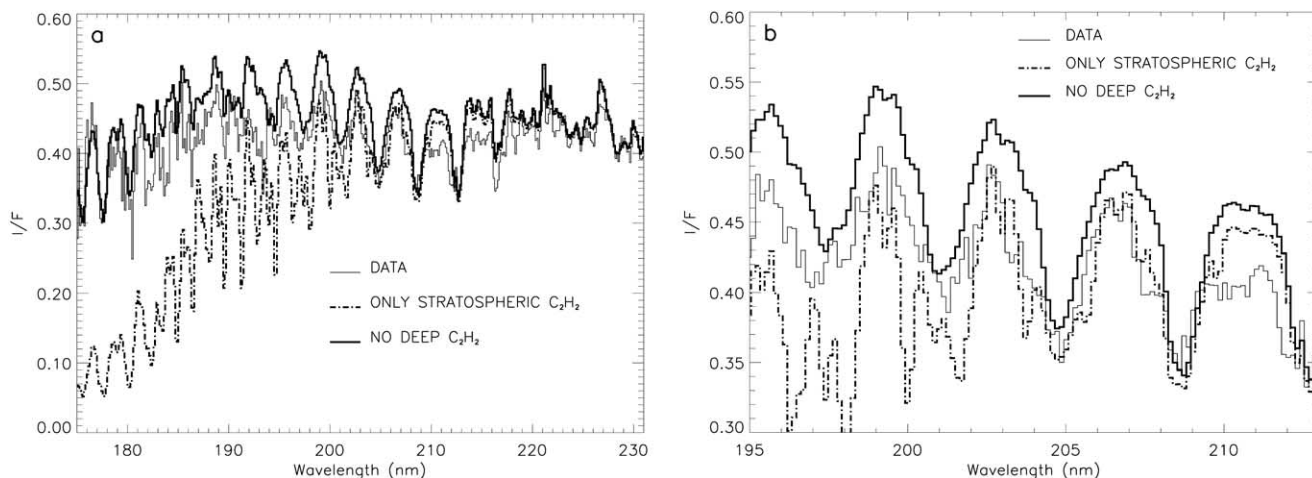


Fig. 9. Comparison of the data with the I/F resulting from variations of model D. (a) The entire useful spectral range of the FOS spectrum is shown. (b) The observed and model spectra are displayed only from wavelengths of 195.0 to 203.0 nm to focus on the long-wavelength acetylene features. The thick dot-dashed line is the I/F obtained when all the  $C_2H_2$  is located in the stratosphere from 0 to 60 mbar with a constant mole fraction of  $3 \times 10^{-7}$ . This distribution reproduces the features above 205 nm, but below 200 nm the I/F is much darker than the data. However, even though acetylene features from this model are too strong, panel b clearly shows that the structure overlying the ammonia bands is due to acetylene. The thick solid line is the I/F obtained when the acetylene profile of Table 6 is used in conjunction with the ammonia profile and haze distribution and optical properties of model D. The modeled ammonia features are much smoother than the data and do not exhibit any substantial acetylene signature above 195.0 nm.

wavelengths in the ultraviolet are needed to analyze jovian spectra accurately.

Finally, and most interestingly, the presence of acetylene features longward of 200.0 nm cannot be explained solely with the presence of stratospheric  $C_2H_2$ : A substantial abundance of tropospheric  $C_2H_2$  is implied by the data. It is possible to separate the influence of stratospheric and tropospheric acetylene using the broad wavelength range and high signal-to-noise ratio at long wavelengths of the FOS data. The shorter wavelengths, below approximately 200 nm, constrain the  $C_2H_2$  column abundance in the stratosphere. This is illustrated in Fig. 8b, based on the atmospheric model of Table 6, which is consistent with past analyses of ultraviolet observations. Although the model appears to match wavelengths below 200 nm fairly well, it fails in two ways at longer wavelengths. First, the shape of what appear to be predominantly ammonia bands is not well fit. The model I/F is high relative to the observations at 203.5, 206.7, and 207.5 nm, as shown in the figure. This occurs because these features are produced by a combination of  $NH_3$  and  $C_2H_2$ , not  $NH_3$  alone. This is demonstrated in Figs. 9a and 9b, which show that  $C_2H_2$  has a large influence on the shape of the bands in just the manner observed in the data. The observed bands have a peaked shape whereas models with only ammonia produce a much smoother profile. The peaked shape is due to the influence of acetylene absorption in the wings of the ammonia bands.

Figs. 9a and 9b clearly establish that the spectrum in the 200- to 210-nm region is strongly affected by  $C_2H_2$  absorption. Comparison with the shorter wavelength region of the spectrum requires that the acetylene that affects the 200- to 210-nm region must reside in the troposphere. As shown in Fig. 9a, the 200- to 210-nm region can be fitted with large

amounts of stratospheric  $C_2H_2$ , but then the fit at short wavelengths is exceedingly poor. This happens because the absorption cross section of  $C_2H_2$  is much larger at short wavelengths than in the 200- to 210-nm region. The dual requirements of a modest amount of acetylene for the short-wavelength region and a large amount of acetylene for the long-wavelength region lead to the conclusion that much of the acetylene resides in the troposphere. At these deep levels it lies below the atmospheric regions where the short-wavelength spectrum is established and therefore can influence the long-wavelength regions without affecting the short-wavelength regions.

Table 3 shows the different acetylene vertical distributions that provide an excellent fit to the data. All these models require large abundances of acetylene in the troposphere. In the nominal model, model D, the  $C_2H_2$  mole fraction decreases from the upper to the lower stratosphere as had been previously reported in the literature. At 60 mbar, the  $C_2H_2$  mole fraction starts increasing with pressure until it reaches a plateau of  $1.5 \times 10^{-7}$  at 120 mbar, around the tropopause. At pressures greater than 300 mbar, the acetylene mole fraction is uncertain because its cross section is unknown above 210.0 nm (see Fig. 6). Although the vertical profile of acetylene is assumed to be constant with altitudes at these depths (except in model A), a total absence of acetylene at these pressures can be compensated by increasing the imaginary index of refraction of the stratospheric haze above 210 nm. The I/F produced by model D, shown by the thick solid line in Fig. 6, reproduces well both the short-wavelength and long-wavelength  $C_2H_2$  features of the FOS spectrum up to 210.0 nm, beyond which acetylene cross-section measurements are unavailable. The other models help quantify the uncertainties in the vertical struc-

ture of Jupiter's atmosphere. Model A shows that the mole fraction of acetylene need not be constant below the 120-mbar pressure level. Models B and C explore changes in the  $C_2H_2$  distribution in the 60- to 120-mbar region as well as small changes in the  $NH_3$  distribution. Models E and F concentrate on the 0- to 60-mbar region. Finally, models G and H try to evaluate the uncertainties in the mole fraction of acetylene in the deeper regions of the troposphere, just above the supposed ammonia cloud. Model J only differs from model D in its  $NH_3$  distribution.

The jovian  $C_2H_2$  distribution can also be determined through analysis of acetylene emission features in Jupiter's mid-infrared spectrum. No prior analyses of these features required invoking tropospheric  $C_2H_2$ , although it is not clear that attempts were made to consider this possibility. To determine whether Jupiter's infrared spectrum is consistent with tropospheric  $C_2H_2$ , the  $\nu_5$  fundamental band of  $C_2H_2$  was analyzed.

The  $C_2H_2$  spectrum was recorded on May 16 1995 at NASA's Infrared Telescope Facility using the Irshell spectrometer (the University of Texas mid-IR spectrometer, Lacy et al., 1989). The observation sampled a  $3 \times 3$ -arc-second region centered at  $2^\circ$  latitude on the central meridian. The synthetic spectra were computed with line-by-line calculations based on line positions, energy levels, and strengths from the GEISA database (Husson et al., 1991). This calculation assumes the  $C_2H_2$  distribution of model D for pressures higher than 20 mbar. At lower pressures, a distribution simultaneously consistent with the 0- to 20-mbar column abundance of model D and with the results from Noll et al. (1986), Sada et al. (1998), and Yelle et al. (2001) is adopted. This calculation also assumes a thermal profile formed from a smoothed Galileo/ASI profile at pressures lower than 0.1 bar (Yelle et al., 2001) and a thermal profile from the SEB for pressures greater than 0.1 bar [derived following the techniques of Griffith et al. (1992)]. As shown in Fig. 10, the additional opacity in the troposphere depresses the wings of the  $C_2H_2$  band below the observed continuum level.

Both the  $C_2H_2$  distribution and the thermal profile establish the shape of the band upon the 125-K brightness temperature continuum. The center of the band is optically thick at 0.03 bar and emission emanates from this level and above, where temperatures exceed 125 K. From the 0.03-bar to the 0.2-bar level the ambient temperature decreases (by 10 K in the assumed temperature profile) and the overlying column abundance increases by a factor of 20. Emissions originate from these deeper and cooler levels in the wings of the band. Since the continuum is formed by pressure-induced  $H_2$  and He absorption, deeper in the atmosphere ( $\sim 0.3$ -bar level) where the temperatures are higher, the wings appear as absorption features relative to the continuum. One should note that the thermal profile used is likely warmer than that pertinent to the region sampled by the spectrum. Yet, an absorptive wing will form in a cooler

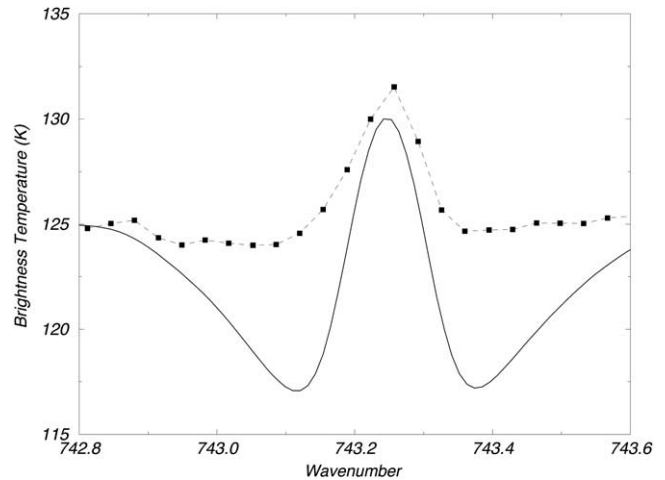


Fig. 10. Jovian  $\nu_5$  fundamental band of  $C_2H_2$ . The wings of the modeled line profile (solid line) are depressed well below the continuum level of the data (squares connected by the dashed line) because of the additional  $C_2H_2$  opacity in the colder regions near the tropopause. See text for a description of the model.

thermal profile as long as the continuum emission derives from the hotter levels below the tropopause.

It is not clear how to reconcile the ultraviolet and infrared observations. The mismatch between the infrared models and the data occurs because an additional opacity source was added in the troposphere, where atmospheric temperatures are coldest. It is important however to recognize that all observations are spatially averaged over a considerable area on Jupiter's disk. The ultraviolet and infrared observations sample the area very differently, with the infrared observations particularly sensitive to the warmer regions. If  $C_2H_2$  resided in hot upwelling regions, where the tropospheric temperatures are warmer than average, the wings might be at the same brightness temperature as the continuum.

Another possibility is the existence of opacity in the stratosphere near the temperature characteristic of the infrared continuum, 125 K. Such an opacity would have to be due to large aerosols; however, there is no reason to expect such aerosols and no other observational evidence suggestive of their existence could be found. As far as the ultraviolet observations are concerned, one should remain aware that the laboratory cross sections used in this analysis have been measured at temperatures higher than those found on Jupiter. Since the contrast of the absorption bands in the  $C_2H_2$  cross section increases with decreasing temperature it may require less  $C_2H_2$  to match the features in the 200- to 210-nm range than is found in this analysis. This would reduce but probably not eliminate the amount of tropospheric acetylene required to fit the observations. Finally, the ultraviolet and infrared observations shown here were made at different times and pertain to different locations on Jupiter. It is possible that the acetylene abundance in Jupiter's troposphere varies strongly with time or location. Co-

ordinated and simultaneous ultraviolet and infrared observations would be very helpful to further explore this problem. Whatever the explanation may be, the acetylene vertical distribution derived from the ultraviolet spectrum remains to be explained in terms of physical processes.

## 5. Conclusions

The following conclusions were reached from an analysis of an ultraviolet equatorial spectrum of the jovian atmosphere obtained with the FOS:

1. An acetylene mole fraction of about  $1.5 \times 10^{-7}$  is inferred in the upper troposphere, from 120 to 300 mbar, from the first detailed analysis of acetylene absorption features between 190.0 and 210.0 nm. This is an enhancement by about a factor of 4 compared to the acetylene abundances in the 60- to 80-mbar pressure region.
2. The presence of acetylene in Jupiter's troposphere cannot at this time be reconciled with observations in the infrared. Simultaneous ultraviolet and infrared observations of the same location in Jupiter's troposphere are needed to address this issue.
3. Ammonia seems to be highly undersaturated, but this conclusion may result from use of an ammonia cross section measured at a temperature significantly higher (175 K) than exists in the upper troposphere (110–140 K).
4. Ammonia clouds are allowed by the spectrum only if they are strong scatterers in the ultraviolet. The dark tropospheric cloud of Wagener et al. (1985) is inconsistent with the amplitude of the Raman features seen in the spectrum.
5. The large amplitude of the Raman features observed in the spectrum demonstrates that haze (or unknown molecular absorbers) located in the stratosphere, not the troposphere, are responsible for the reflectivity of the jovian atmosphere from 220.0 to 232.0 nm.
6. The stratospheric haze seemingly displays a sudden increase in its imaginary index of refraction by a factor of about 25 with increasing wavelength around 201.0 nm. However, this probably results from the combination of the haze with an unaccounted absorber that absorbs at these longer wavelengths.

The improvements in the quality of ultraviolet spectra of Jupiter made possible by HST have required the development of the more sophisticated analysis tools described here. The limiting factor in the analysis of these spectra is now found to be laboratory data on ultraviolet cross sections. High-resolution measurements, at temperatures appropriate for the lower stratosphere and upper troposphere are needed for ammonia, various hydrocarbons, nitriles, and amides above 210.0 nm, to be able to accurately interpret existing data.

## Acknowledgments

Support for this work was provided by NASA Grant NAG5-4426 and through Grant AR-08008.01-96A from the Space Telescope Science Institute, which is operated by AURA, Inc., under NASA Contract NAS 5-26555.

## References

- Anderson, J.D., 1976. The gravity field of Jupiter, in: Gehrels, T. (Ed.), *Jupiter*, University of Arizona Press, Tucson, pp. 113–121.
- Bar-Nun, A., Kleinfeld, I., Ganor, E., 1988. Shape and optical properties of aerosols formed by photolysis of acetylene, ethylene, and hydrogen cyanide. *J. Geophys. Res.* 93, 8383–8387.
- Bénilan, Y., Smith, N., Jolly, A., Raulin, F., 2000. The long wavelength range temperature variations of the mid-UV acetylene absorption coefficient. *Planet. Space Sci.* 48, 463–471.
- Bétrémieux, Y., Yelle, R.V., 1999. HST detection of H<sub>2</sub> Raman scattering in the jovian atmosphere. *Icarus* 142, 324–341.
- Bézar, B., Griffith, C.A., Kelly, D.M., Lacy, J.H., Greathouse, T., Orton, G., 1997. Thermal infrared imaging spectroscopy of Shoemaker–Levy 9 impact sites: temperature and HCN retrievals. *Icarus* 125, 94–120.
- Bjoraker, G.L., Larson, H.P., Kunde, V.G., 1986. The abundance and distribution of water vapor in Jupiter's atmosphere. *Astrophys. J.* 311, 1058–1072.
- Carlson, B.E., Lacy, A.A., Rossow, W.B., 1993. Tropospheric gas composition and cloud structure of the jovian north equatorial belt. *J. Geophys. Res.* 98, 5251–5290.
- Carlson, B.E., Lacy, A.A., Rossow, W.B., 1994. Belt-zone variations in the jovian cloud structure. *J. Geophys. Res.* 99, 14623–14658.
- Chen, F., Judge, D.L., Wu, C.Y.R., Caldwell, J.J., White, H.P., Wagener, R., 1991. High-resolution, low temperature photoabsorption cross sections of C<sub>2</sub>H<sub>2</sub>, PH<sub>3</sub>, AsH<sub>3</sub>, and GeH<sub>4</sub>, with applications to Saturn's atmosphere. *J. Geophys. Res.* 96, 17519–17527.
- Chen, F., Judge, D.L., Wu, C.Y.R., Caldwell, J.J., 1999. Low and room temperature photoabsorption cross sections of NH<sub>3</sub> in the UV region. *Planet. Space Sci.* 47, 261–266.
- Clarke, J.T., Moos, H.W., Feldman, P.D., 1982. The far-ultraviolet spectra and geometric albedos of Jupiter and Saturn. *Astrophys. J.* 255, 806–818.
- Combes, M., Courtin, R., Caldwell, J., Encrenaz, T., Fricke, K.H., Moore, V., Owen, T., Butterworth, P.S., 1981. Vertical distribution of NH<sub>3</sub> in the upper jovian atmosphere from IUE observations. *Adv. Space Res.* 1, 169–175.
- Dick, K.A., Ziko, A.O., 1973. Ammonia absorption relevant to the albedo of Jupiter. I. Experimental results. *Astrophys. J.* 182, 609–613.
- Edgington, S.G., Atreya, S.K., Trafton, L.M., Caldwell, J.J., Beebe, R.F., Simon, A.A., West, R.A., Barnet, C., 1998. On the latitude variation of ammonia, acetylene, and phosphine altitude profile on Jupiter from HST Faint Object Spectrograph observations. *Icarus* 133, 192–209.
- Encrenaz, T., de Graauw, T., Schaeidt, S., Lellouche, E., Feuchtgruber, H., Beintema, D.A., Bézar, B., Drossart, P., Griffin, M., Heras, A., Kessler, M., Leech, K., Morris, P., Roelfsema, P.R., Roos-Serote, M., Salama, A., Vandenbussche, B., Valentijn, E.A., Davis, G.R., Naylor, D.A., 1996. First results of ISO-SWS observations of Jupiter. *Astron. Astrophys.* 315, L397–400.
- Ferris, J.P., Ishikawa, Y., 1988. Formation of HCN and acetylene oligomers by photolysis of ammonia in the presence of acetylene: applications to the atmospheric chemistry of Jupiter. *J. Am. Chem. Soc.* 110, 4306–4312.
- Fouchet, T., Lellouche, E., Bézar, B., Encrenaz, T., Drossart, P., Feuchtgruber, H., de Graauw, T., 2000. ISO-SWS observation of Jupiter: measurement of the ammonia tropospheric profile and of the <sup>15</sup>N/<sup>14</sup>N isotropic ratio. *Icarus* 143, 223–243.

- Gierasch, P.J., Conrath, B.J., Magalhães, J.A., 1986. Zonal mean properties of Jupiter's upper troposphere from Voyager infrared observations. *Icarus* 67, 456–483.
- Gladstone, G.R., Yung, Y.L., 1983. An analysis of the reflection spectrum of Jupiter from 1500Å to 1740Å. *Astrophys. J.* 266, 415–424.
- Griffith, C.A., Bézard, B., Owen, T., Gautier, D., 1992. The tropospheric abundances of NH<sub>3</sub> and PH<sub>3</sub> in Jupiter's great red spot, from Voyager IRIS observations. *Icarus* 98, 82–93.
- Husson, N., Bonnet, B., Scott, N.N., Chédin, A., 1991. The GEISA data bank 1991 version. Internal note L.M.D. 163, Laboratoire de Météorologie Dynamique, Plaiseau, France.
- Kaminski, J.W., McConnell, J.C., 1991. A note on the enhancement of J values in optically thick scattering atmospheres. *Can. J. Phys.* 69, 1166–1174.
- Kaye, J.A., Strobel, D.E., 1983. HCN formation on Jupiter. The coupled photochemistry of ammonia and acetylene. *Icarus* 54, 417–433.
- Kunde, V., Hanel, R., Maguire, W., Gautier, D., Baluteau, J.P., Marten, A., Chedin, A., Husson, N., Scott, N., 1982. The tropospheric gas composition of Jupiter's north equatorial belt (NH<sub>3</sub>, PH<sub>3</sub>, CH<sub>3</sub>D, GeH<sub>4</sub>, H<sub>2</sub>O) and the jovian D/H isotopic ratio. *Astrophys. J.* 263, 443–467.
- Lacy, J.H., Achterman, J.M., Bruce, D.E., Lester, D.F., Arens, J.F., Peck, M.C., Gaalema, S.D., 1989. Irshell: a mid-infrared cryogenic echelle spectrograph. *Publ. Astron. Soc. Pac.* 101, 1166–1175.
- Lara, L.-M., Bézard, B., Griffith, C.A., Lacy, J.H., Owen, T., 1998. High-resolution 10-micrometer spectroscopy of ammonia and phosphine lines on Jupiter. *Icarus* 131, 317–333.
- Larson, L.E., Mickelson, M.E., 1993. The temperature dependent absorption coefficient for methane at 5430 Å and 6190 Å. Fifth International Conference on Laboratory Research for Planetary Atmospheres, Boulder, CO, 17 October 1993.
- Lellouch, E., Drossart, P., Encrenaz, T., 1989. A new analysis of the jovian 5-μm Voyager/IRIS spectra. *Icarus* 77, 457–465.
- Marten, A., Rouan, D., Baluteau, J.P., Gautier, D., Conrath, B.J., Hanel, R.A., Kunde, V., Samuelson, R., Chedin, A., Scott, N., 1981. Study of the ammonia ice cloud layer in the equatorial region of Jupiter from the infrared interferometric experiment on Voyager. *Icarus* 46, 233–248.
- McGrath, M.A., Ballester, G.E., Moos, H.W., 1990. Jovian H<sub>2</sub> dayglow emission (1978–1989). *J. Geophys. Res.* 95, 10365–10373.
- Morrissey, P.F., Feldman, P.D., McGrath, M.A., Wolven, B.C., Moos, H.W., 1995. The ultraviolet reflectivity of Jupiter at 3.5Å resolution from Astro-1 and Astro-2. *Astrophys. J.* 454, L65–68.
- Niemann, H.B., Atreya, S.K., Carignan, G.R., Donahue, T.M., Haberman, J.A., Harpold, D.N., Hartle, R.E., Hunten, D.M., Kasprzak, W.T., Mahaffy, P.R., Owen, T.B., Spencer, N.W., Way, S.H., 1996. The Galileo probe mass spectrometer: composition of Jupiter's atmosphere. *Science* 272, 846–849.
- Niemann, H.B., Atreya, S.K., Carignan, G.R., Donahue, T.M., Haberman, J.A., Harpold, D.N., Hartle, R.E., Hunten, D.M., Kasprzak, W.T., Mahaffy, P.R., Owen, T.C., Way, S.H., 1998. The composition of the jovian atmosphere as determined by the Galileo probe mass spectrometer. *J. Geophys. Res.* 103, 22831–22845.
- Noll, K.S., Knacke, R.F., Tokunaga, A.T., Lacy, J.H., Beck, S., Serabyn, E., 1986. The abundances of ethane and acetylene in the atmospheres of Jupiter and Saturn. *Icarus* 65, 257–263.
- Noy, N., Bar-Nun, A., Podolak, M., 1979. Acetylene photopolymers in Jupiter's stratosphere. *Icarus* 40, 199–204.
- Owen, T., Caldwell, J., Rivolo, A.R., Moore, V., Lane, A.L., Sagan, C., Hunt, G., Ponnamperna, C., 1980. Observations of the spectrum of Jupiter from 1500 to 2000 Å with the IUE. *Astrophys. J.* 236, L39–42.
- Pope, S.K., Tomasko, M.G., Williams, M.S., Perry, M.L., Doose, L.R., Smith, P.H., 1992. Clouds of ammonia ice: laboratory measurements of the single-scattering properties. *Icarus* 100, 203–220.
- Sada, P.V., Bjoraker, G.L., Jennings, D.E., McCabe, G.H., Romani, P.N., 1998. Observations of CH<sub>4</sub>, C<sub>2</sub>H<sub>6</sub>, and C<sub>2</sub>H<sub>2</sub> in the stratosphere of Jupiter. *Icarus* 136, 192–201.
- Seiff, A., Kirk, D.B., Knight, T.C.D., Mihalov, J.D., Blanchard, R.C., Young, R.E., Schubert, G., von Zahn, U., Lehmacher, G., Milos, F.S., Wang, J., 1996. Structure of the atmosphere of Jupiter: Galileo probe measurements. *Science* 272, 844–845.
- Seiff, A., Kirk, D.B., Knight, T.C.D., Young, R.E., Mihalov, J.D., Young, L.A., Milos, F.S., Schubert, G., Blanchard, R.C., Atkinson, D., 1998. Thermal structure of Jupiter's atmosphere near the edge of a 5-μ hot spot in the north equatorial belt. *J. Geophys. Res.* 103, 22857–22889.
- Smith, N.S., Bénilan, Y., Bruston, P., 1998. The temperature dependent absorption cross sections of C<sub>4</sub>H<sub>2</sub> at mid ultraviolet wavelengths. *Planet. Space Sci.* 46, 1215–1220.
- Smith, W.M.H., Conner, C.P., Baines, K.H., 1990. Absorption coefficients for the 6190-Å CH<sub>4</sub> band between 290 and 100 K with application to Uranus' atmosphere. *Icarus* 85, 58–64.
- Strobel, D.F., 1969. The photochemistry of methane in the jovian atmosphere. *J. Atmos. Sci.* 26, 906–911.
- Tokunaga, A.T., Knacke, R.F., Ridgway, S.T., 1980. High spatial and spectral resolution 10-μm observations of Jupiter. *Icarus* 44, 93–101.
- Tomasko, M.G., 1974. Ammonia absorption relevant to the albedo of Jupiter. II. Interpretation. *Astrophys. J.* 187, 641–650.
- Tomasko, M.G., West, R.A., Castillo, N.D., 1978. Photometry and polarimetry of Jupiter at large phase angles. I. Analysis of imaging data of a prominent belt and a zone from Pioneer 10. *Icarus* 33, 558–592.
- Tomasko, M.G., Karkoschka, E., Martinek, S., 1986. Observations of the limb darkening of Jupiter at ultraviolet wavelengths and constraints on the properties and distribution of stratospheric aerosols. *Icarus* 65, 218–243.
- Wagner, R., Caldwell, J., Owen, T., Kim, S.-J., Encrenaz, T., Combes, M., 1985. The jovian stratosphere in the ultraviolet. *Icarus* 63, 222–236.
- West, R.A., Strobel, D.F., Tomasko, M.G., 1986. Clouds, aerosols, and photochemistry in the jovian atmosphere. *Icarus* 65, 161–217.
- Yelle, R.V., McGrath, M.A., 1996. Ultraviolet spectroscopy of the SL9 impact sites. I. The 175–230 nm region. *Icarus* 119, 90–111.
- Yelle, R.V., Griffith, C.A., Young, L.A., 2001. Structure of the jovian stratosphere at the Galileo probe entry site. *Icarus* 152, 331–346.